

SCIENTIFIC REPORTS

OPEN

Extreme sensitivity of the electric-field-induced band gap to the electronic topological transition in sliding bilayer graphene

Kyu Won Lee & Cheol Eui Lee

Received: 19 August 2015

Accepted: 30 October 2015

Published: 04 December 2015

We have investigated the effect of electronic topological transition on the electric field-induced band gap in sliding bilayer graphene by using the density functional theory calculations. The electric field-induced band gap was found to be extremely sensitive to the electronic topological transition. At the electronic topological transition induced by layer sliding, four Dirac cones in the Bernal-stacked bilayer graphene reduces to two Dirac cones with equal or unequal Dirac energies depending on the sliding direction. While the critical electric field required for the band gap opening increases with increasing lateral shift for the two Dirac cones with unequal Dirac energies, the critical field is essentially zero with or without a lateral shift for the two Dirac cones with equal Dirac energies. The critical field is determined by the Dirac energy difference and the electronic screening effect. The electronic screening effect was also found to be enhanced with increasing lateral shift, apparently indicating that the massless helical and massive chiral fermions are responsible for the perfect and imperfect electronic screening, respectively.

Bilayer graphene (BLG) has been recently predicted to undergo an electronic topological transition under a tiny lateral interlayer shift, which may alter the physical properties of BLG significantly¹. At the electronic topological transition induced by layer sliding, four Dirac cones in the AB-stacked BLG reduces to two Dirac cones with equal or unequal Dirac energies depending on the sliding direction¹. A tiny lateral shift, little modifying the binding energy and the interlayer distance of the AB-stacked BLG, is expected to occur easily in real samples¹. Stacking faults by layer sliding were found in recent experiments on BLG grown by chemical vapor deposition at the domain walls between two ideally stacked graphene systems^{2–4}, and sliding of graphene flakes may be initiated by the scanning tunneling microscopy tip⁵. The optimal configuration of the BLG nanoribbons has recently been reported to have a lateral shift between the layers⁶.

On the other hand, the band gap in BLG can be controlled by an external electric field perpendicular to the layer^{7–10}, providing a very useful way for graphene field effect devices. While an anomalous optical phonon splitting in sliding BLG may be utilized to detect tiny misalignment of graphene layers by using the spectroscopic tools¹¹, the effect of layer sliding on the electric field-induced band gap in BLG, which is crucial for the characterization and application of the gated BLG, need to be clarified. Here, our density functional theory (DFT) calculations show that the electric field-induced band gap is extremely sensitive to the electronic topological transition induced by layer sliding in BLG. While the critical electric field required for the band gap opening increases with increasing lateral shift for the two Dirac cones with unequal Dirac energies, the critical field remains essentially zero even with a lateral shift for the two Dirac cones with equal Dirac energies.

The AB and BA stackings, the Bernal stackings, are equivalent to each other, with the carbon atoms of a layer residing on top of a carbon atom or a hollow center of the other layer. In the AA stacking, all

Department of Physics, Korea University, Seoul 136-713, Korea. Correspondence and requests for materials should be addressed to C.E.L. (email: rscel@korea.ac.kr)

the carbon atoms of a layer reside on top of the carbon atoms of the other layer and, in the AA' stacking, all the carbon atoms of a layer reside on the hollow of the other layer¹². The electronic structure of AB-stacked BLG has a quadratic energy dispersion around the K point of the first Brillouin zone, which changes to four Dirac cones with linear dispersions in the very near neighbor of the K point¹³. The electronic structures of AA- and AA'-stacked BLG have just two Dirac cones with unequal Dirac energies around the K point¹². The Dirac energy and the Dirac point respectively indicate the energy and the wavevector when the upper and lower cones are in contact. In the AA stacking, two vertical Dirac cones with unequal Dirac energies have the same Dirac point and, in the AA' stacking, two nonvertical Dirac cones with unequal Dirac energies have different Dirac points¹².

A tiny lateral interlayer shift in the AB-stacked BLG has been predicted to induce an electronic topological transitions in the low energy electronic structure, conserving the quadratic energy dispersion at a relatively high energy¹. As the lateral shift increases further along the armchair direction, which is the shortest path from the AB to the BA stacking, the AB stacking changes to the AA or AA' stacking, where the quadratic dispersion disappears¹². Since the BA stacking is equivalent to the AB stacking, the lateral shift can be taken to occur along the path from the AB to the AA stacking or to the AA' stacking. In this work, our DFT calculations show that the electronic screening effect increases with increasing lateral shift and, finally, the electric field would be perfectly screened in the AA and AA' stackings, possibly indicating that the massless helical and massive chiral fermions are responsible for the perfect and imperfect electronic screening, respectively. Also, the critical electric field required for the band gap opening appears to be determined by the Dirac energy difference and the electronic screening effect.

Figure 1 shows the atomic geometry and the energy map for the valence band near the K point of the Brillouin zone. Fig. 1a,b correspond to AB-stacked BLG. Considering the low energy electronic structure of AB-stacked BLG^{1,13}, four Dirac cones are formed around the Fermi level at the Dirac points of \vec{k}_{D0} , \vec{k}_{D1} , \vec{k}_{D2} , and \vec{k}_{D3} as shown in Fig. 1b. Figure 1c–f correspond to sliding BLG. In this work, the lower layer slides with respect to the fixed upper layer along the y -axis corresponding to the armchair direction as shown in Fig. 1c,e, which is described by a sliding vector $\vec{d}_s = d_s \hat{y}$. Figure 1c,d correspond to sliding BLG with $d_s = +0.24 \text{ \AA}$, and Fig. 1e,f correspond to sliding BLG with $d_s = -0.24 \text{ \AA}$. In Fig. 1c,e, the top and side views of sliding BLG are shown on the left and right, and the sliding direction of lower layer is indicated by arrows. AB-stacked BLG corresponds to $d_s = 0$. With the C-C bond length $a_c = 1.42 \text{ \AA}$, $d_s = a_c$ or $d_s = -2a_c$ give a BA stacking. On the other hand, $d_s = 0.5a_c$ and $d_s = -a_c$ give an AA' and an AA stacking, respectively¹². Thus, the layer sliding occurs along the path from the AB to the AA' stacking when $d_s > 0$ or along the path from the AB to the AA stacking when $d_s < 0$. The layer sliding along the y -axis includes the two electronic topological transitions predicted in previous works¹. When $d_s \gtrsim +0.012 \text{ \AA}$, the three Dirac cones at \vec{k}_{D1} , \vec{k}_{D2} , and \vec{k}_{D3} collapse into a single Dirac cones as shown in Fig. 1d. When $d_s \lesssim -0.004 \text{ \AA}$, the two Dirac cones at \vec{k}_{D0} and \vec{k}_{D1} meet and disappear leaving only two Dirac cones at \vec{k}_{D2} and \vec{k}_{D3} as shown in Fig. 1f. While the energy maxima in Fig. 1d corresponding to the Dirac energy show a difference between the Dirac cones at \vec{k}_{D0} and \vec{k}_{D1} , the maxima in Fig. 1f show no difference between the Dirac cones at \vec{k}_{D2} and \vec{k}_{D3} ¹. The electronic topological transition induced by layer sliding leads to two Dirac cones with equal or unequal Dirac energies depending on the sliding direction^{1,12}, significantly changing the physical properties of BLG as will be discussed below.

Figure 2 shows the electric field-induced band gap obtained from the band structure and density of states (DOS) as a function of the electric field F_z perpendicular to the layer. In the AB-stacked BLG, the critical electric field F_c required for the band gap opening was about 10 mV/nm, as in previous works¹⁴. Figure 2a,b show the electric-field induced band gap when the layer sliding occurs along the path from the AB to the AA' stacking ($d_s > 0$) and when the layer sliding occurs along the path from the AB to the AA stacking ($d_s < 0$), respectively. The most notable is that, while the critical field F_c increases with increasing lateral shift along the path from the AB to the AA' stacking ($d_s > 0$, see Fig. 2a), the critical field F_c was less than 10 mV/nm and is believed to be essentially zero for any lateral shift along the path from the AB to the AA stacking ($d_s < 0$, see Fig. 2b). In other words, the critical field increases with increasing lateral shift for the two Dirac cones with unequal Dirac energies but is essentially zero with or without a lateral shift for the two Dirac cones with equal Dirac energies. The electric field-induced band gap is extremely sensitive to the electronic topological transition induced by layer sliding, which can be utilized to characterize the gated BLG and may be responsible for the contradicting results in recent experiments on the gated BLG^{15–19}.

Figure 3 shows the band structures and DOS near the K point. In each panel, the band structure and DOS are shown on the left and right, respectively. The DOS of sliding BLG exhibits symmetric peaks around the Fermi level caused by the saddle points between the two Dirac cones, consistently with a previous work¹². Figure 3a,b show the band structure at $F_z = 1$ and 3 V/nm, respectively, when $d_s = +0.24 \text{ \AA}$. The layer sliding along the path from the AB to the AA' stacking ($d_s > 0$) produces two Dirac cones with unequal Dirac energies (see Fig. 1d). As shown in Fig. 3a, at $F_z = 1 \text{ V/nm}$, an energy gap ε opens at the Dirac points but there is no band gap since ε is still smaller than the Dirac energy difference δE_D between the two Dirac cones. As shown in Fig. 3b, at $F_z = 3 \text{ V/nm}$, ε larger than δE_D leads to a band gap E_g . When $d_s > 0$, the electric field-induced energy gap ε must exceed the Dirac energy difference in order to open a band gap, leading to a finite critical field. On the other hand, the layer sliding along the path

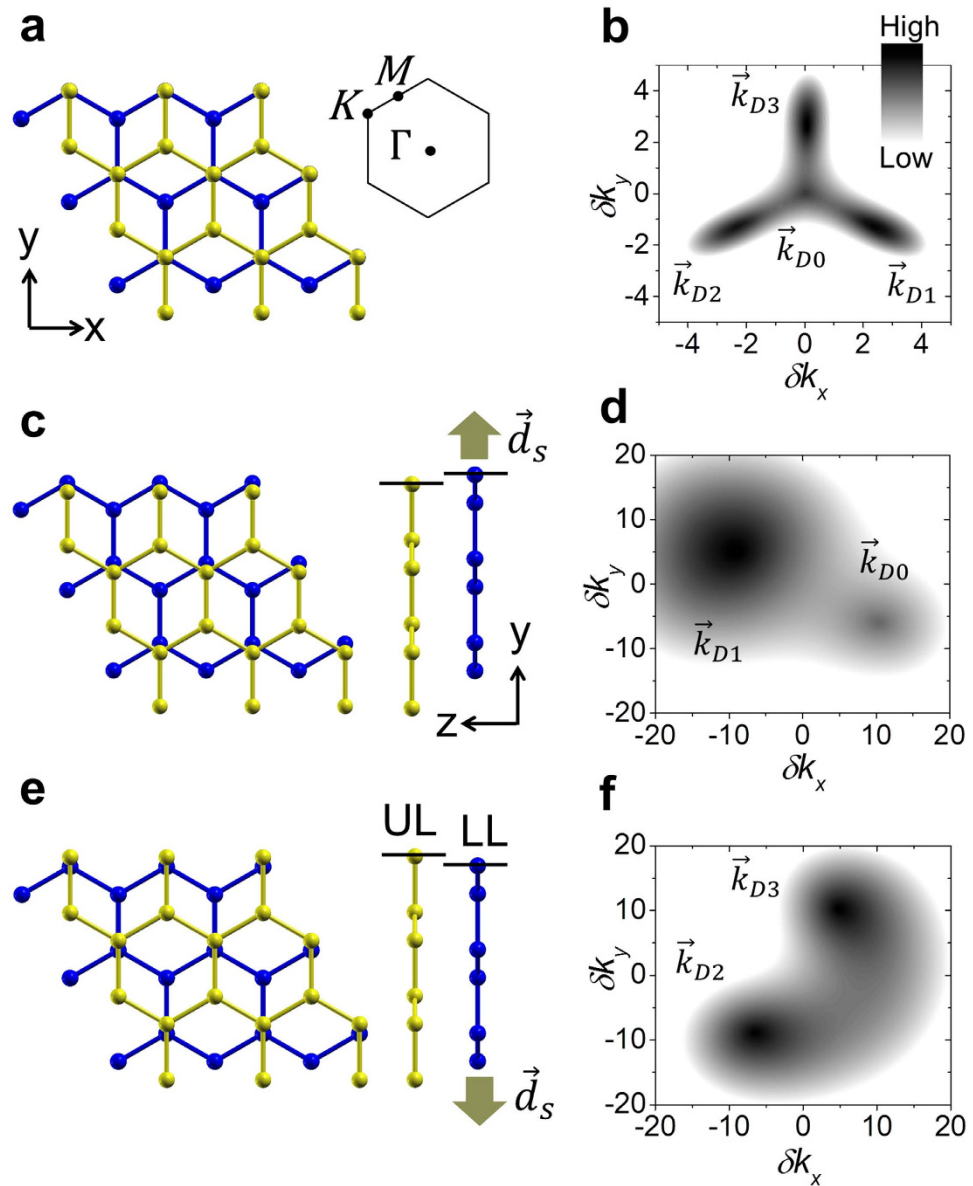


Figure 1. Atomic geometry and energy map for the valence band near the K point. (a) Atomic geometry of AB-stacked BLG. Blue and yellow spheres correspond to the carbon atoms in the lower and upper layers, respectively. Inset shows the first Brillouin zone and the symmetric points of Γ , M and K . (b) Energy map for the valence band of AB-stacked BLG. $\delta \vec{k} = (\delta k_x, \delta k_y) = 1000(\vec{k} - K)$ in units of $2\pi/a$ and high energy appears dark. The darkest spots (energy maxima) correspond to four Dirac cones at the Dirac points of \vec{k}_{D0} , \vec{k}_{D1} , \vec{k}_{D2} and \vec{k}_{D3} . Panels (c,d) show the atomic geometry and the energy map for the valence band of sliding BLG with $d_s = +0.24 \text{ \AA}$, respectively. Panels (e,f) show the atomic geometry and the energy map for the valence band of sliding BLG with $d_s = -0.24 \text{ \AA}$, respectively. In panels (c,e), The top and side views are shown on the left and right, respectively, and the arrows indicate the sliding direction of the lower layer (LL) with respect to the fixed upper layer (UL).

from the AB to the AA stacking produces two Dirac cones with equal Dirac energies (see Fig. 1f) and the electric field-induced energy gap ε , even if infinitesimally small, directly leads to a band gap when $d_s < 0$ as shown in Fig. 3c,d. The results will be further discussed below. Thus, the electronic phase produced by a layer sliding along the path from the AB to the AA stacking is believed to be very sensitive to a perturbation such as spin-orbit interaction or the substrate.

As can be seen in Fig. 2, the band gap is quite linear to the electric field F_z . In the tight binding model for the AB-stacked BLG¹³, the electrostatic potential energy difference U between the two layers gives rise to a band gap $E_g = \gamma_1 U / \sqrt{\gamma_1^2 + U^2}$ with the nearest neighbor interlayer hopping parameter γ_1 . For a large $U \gg \gamma_1$, the band gap has a saturation value, $E_g = \gamma_1$. For a small $U \ll \gamma_1$, the band gap is equal

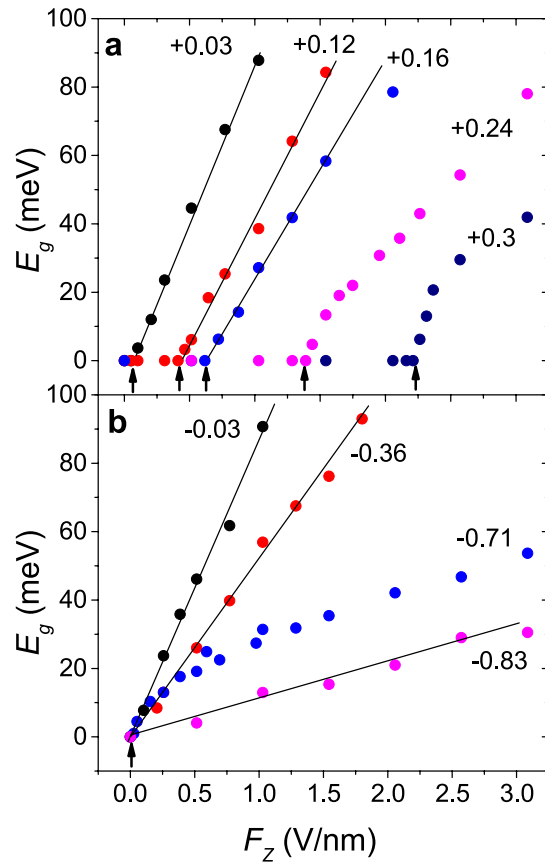


Figure 2. Electric field-induced band gap as a function of electric field F_z . (a) When the layer slides along the path from the AB to the AA' stacking ($d_s > 0$). (b) When the layer slides along the path from the AB to the AA stacking ($d_s < 0$). Numbers indicate d_s in units of Å and arrows indicate the critical field F_c required for the band gap opening. The straight lines are the linear fits as described in the text.

to the potential energy difference, $E_g = U$. The potential energy difference U induced by the electric field F_z under an electronic screening effect can be described as $U = eF_z d_e$. Here, d_e is the effective interlayer distance including the electronic screening effect and was about 1 Å in the AB-stacked BLG¹⁴. d_e equal to the interlayer distance of BLG indicates that there is no screening effect, and $d_e = 0$ indicates that the electric field is perfectly screened and $E_g = U$ for any F_z . Thus, the electric field-induced band gap can be described as $E_g(F_z) \sim eF_z d_e + E_g(0)$, where the offset $E_g(0)$ was added for the Dirac energy difference. The straight lines in Fig. 2 show the linear fits. When $d_s < 0$, the offset $E_g(0)$ was set to zero. E_g is not a simple linear function of F_z around $d_s \sim -0.71$ Å and when $d_s \gtrsim 0.2$ Å (see Fig. 2). When $d_s \gtrsim 0.48$ Å, F_z does not open a band gap because of the critical field high enough to close the energy gap between the Γ and K points even if an energy gap opens at the K point.

Figure 4a,b show d_e and $E_g(0)$, respectively, obtained by the linear fits in Fig. 2. The critical field F_c shown in Fig. 4c was obtained directly from Fig. 2. As shown in Fig. 4a, the effective interlayer distance d_e decreases with increasing d_s and appears to go to zero when d_s goes to $-a_c$ or $+0.5a_c$, each corresponding to the AA and AA' stackings. The results indicate that the electronic screening effects increase as the sliding BLG approaches the AA or AA' stacking. Indeed, we observed that the electric field F_z does not open an energy gap at the Dirac point in the AA' stacking or in the AA stacking, indicating that the electric field is perfectly screened. For $d_s = 0.48$ Å, F_z does not open a band gap but still opens an energy gap increasing with the field at the Dirac points, indicating that the electric field is imperfectly screened. While, in a tight binding model for the AA-stacked BLG²⁰, the electrostatic potential energy difference between the layers has already been reported not to open a band gap, our results indicate that the electric field is perfectly screened in the AA-stacked BLG and thus cannot induce a potential energy difference. The AA and AA' stackings have just two Dirac cones with linear energy dispersion contrasting to the quadratic energy dispersion characteristic of the AB stacking. A previous work²¹ showed that when the AB-stacked BLG is decoupled by an increase of the interlayer distance and the electric field-induced charge redistribution, the electric field cannot open a band gap. Thus, the massless helical fermions with

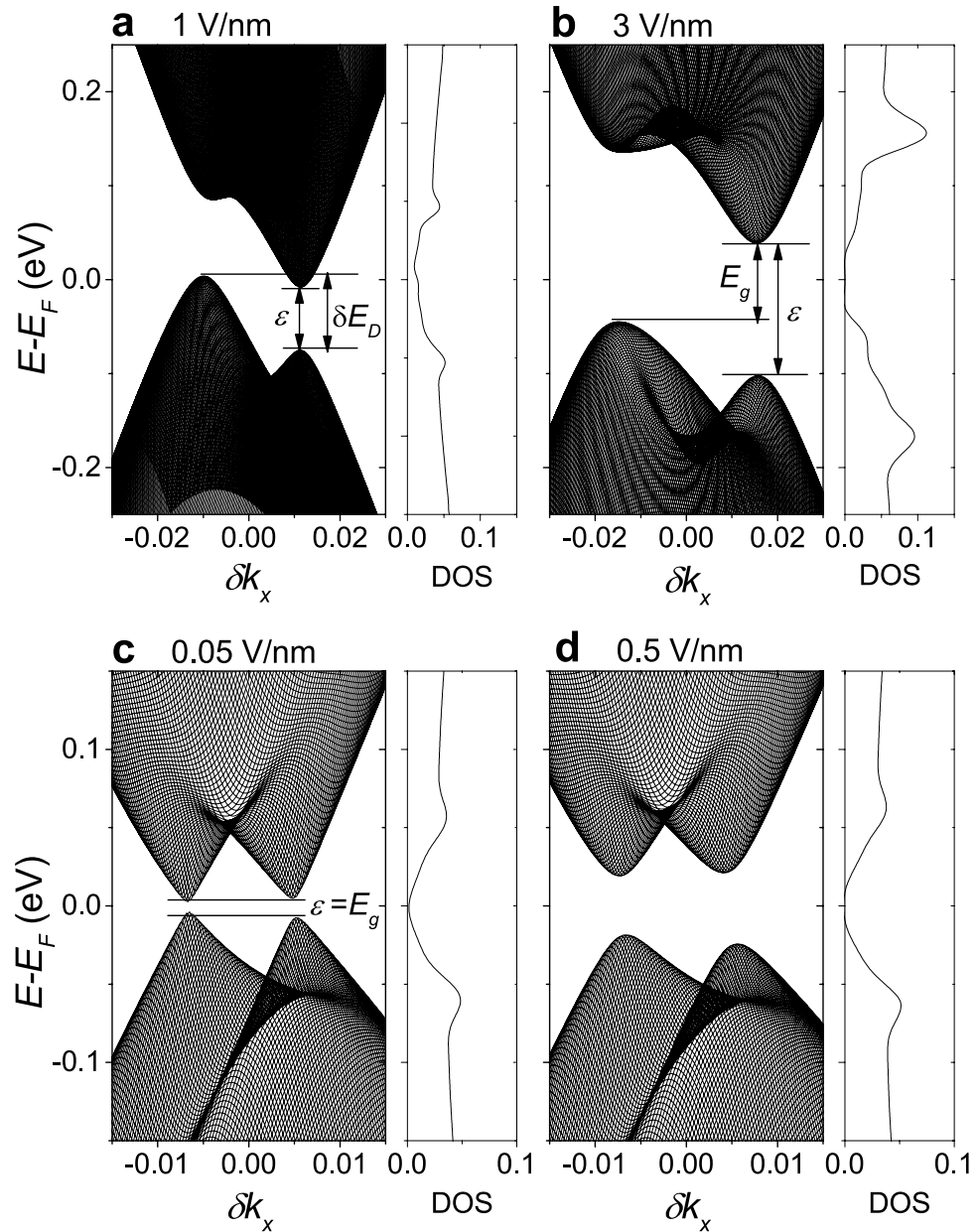


Figure 3. Band structure and density of states near the K point. In each panel, the band structure and density of states (DOS) are shown on the left and right, respectively. The Fermi level E_F was set to zero. Panels (a,b) correspond to $F_z = 1$ and 3 V/nm , respectively, when $d_s = +0.24 \text{ \AA}$. Panels (c,d) correspond to $F_z = 0.05$ and 0.5 V/nm , respectively, when $d_s = -0.24 \text{ \AA}$. DOS was shown in arbitrary units and $\delta \vec{k} = (\delta k_x, \delta k_y) = 1000(\vec{k} - \vec{K})$ in units of $2\pi/a$. When $d_s > 0$, as shown in panels (a,b), the electric field-induced energy gap ε at the Dirac points must exceed the Dirac energy difference δE_D in order to open a band gap E_g . When $d_s < 0$, as shown in panels (c,d), ε is equal to E_g .

a linear energy dispersion would be responsible for the perfect screening while the massive chiral fermions with a quadratic dispersion would be responsible for the imperfect screening.

In Fig. 4b, the Dirac energy difference δE_D between the Dirac cones at \vec{k}_{D0} and \vec{k}_{D1} , which is directly obtained from the energy map for the valence band such as shown in Fig. 1, was compared with $E_g(0)$ obtained by the linear fits in Fig. 2. In a previous tight binding model for the sliding BLG¹, the Dirac energy difference between the Dirac cones at \vec{k}_{D0} and \vec{k}_{D1} was described as $\delta E_D \approx \delta E_D(0)(1 - d_s/0.016)\sqrt{1 + 4d_s/0.016}$ and there is no Dirac energy difference between the Dirac cones at \vec{k}_{D2} and \vec{k}_{D3} . The solid line in Fig. 4b corresponds to the tight binding model description with $\delta E_D(0) = 1 \text{ meV}$, which is consistent with our DFT results. δE_D also agrees well with $E_g(0)$, especially for small d_s . Since the band gap is zero at the critical electric field F_c , indicating that the critical

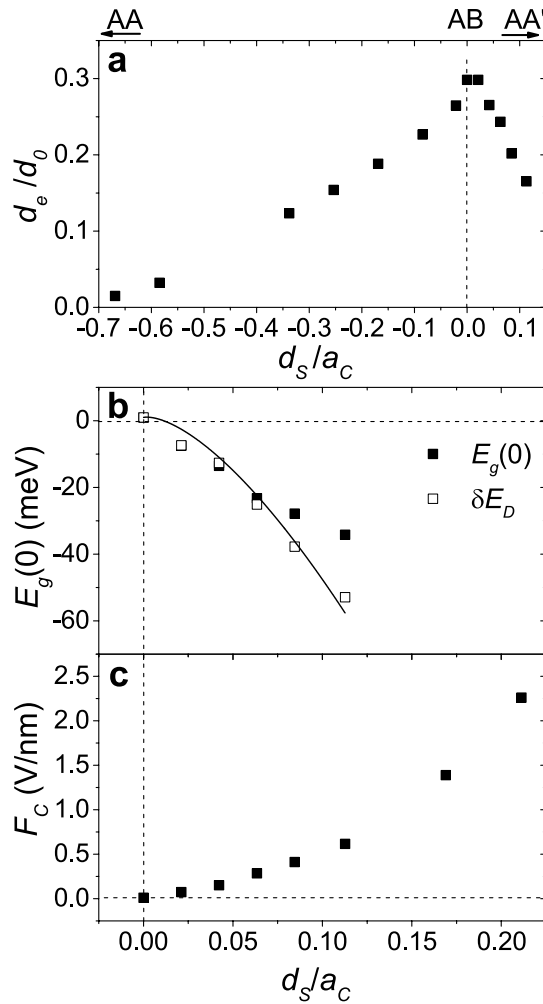


Figure 4. Parameters d_e , $E_g(0)$ and F_c as a function of d_s/a_c . The C-C bond length a_c was set to 1.42 Å. **(a)** Effective interlayer distance d_e normalized to the interlayer distance d_0 of the AB-stacked BLG. **(b)** The offset $E_g(0)$ obtained from the linear fits in Fig. 2 is compared to the Dirac energy difference δE_D obtained from the energy map for the valence band such as shown in Fig. 1. The solid line in panel **(b)** corresponds to the tight binding model description for δE_D as explained in the text. **(c)** Critical electric field F_c obtained directly from Fig. 2.

field $F_c = -E_g(0)/(ed_e)$ is determined by the Dirac energy difference and the electronic screening effects.

Experimental measurements of the band gap in BLG are still controversial^{15–19} and can be affected by a strain²², twist²³, or a lateral shift. We did not find experimental measurements appropriate enough to be compared with our DFT results, however, while preparing this manuscript, a recent tight binding (TB) model study on a similar issue came to our attention²⁴. Since the TB model includes only the first-nearest-interlayer hopping terms²⁴ and the details of the electronic topological transition are determined by the higher-order interlayer hopping terms¹, the electronic topological transition induced by a tiny lateral shift in the AB stacking and its effect on the electric field-induced band gap opening were not investigated in detail in the TB model. Instead, the TB model investigated a lateral shift in AA and AA' stackings, each leading to two Dirac cones with equal and unequal Dirac energies, and the electric field-induced band gap opening was shown to be sensitive to the Dirac energy difference between the two Dirac cones, consistently with our DFT results. Despite the great success of DFT calculations for the electronic properties, the limits of DFT calculations to provide realistic estimation of the band gap have long been known and more realistic estimation of the band gap can be achieved by using the hybrid functionals and GW corrections. However, the essential characteristics of the electric field-induced band gap in sliding BLG, for which our DFT calculations are consistent with a TB model prediction, is believed to be unaffected.

In summary, we have investigated the effect of electronic topological transition on the electric field-induced band gap in BLG by using the DFT calculations. Under a lateral interlayer shift, AB-stacked BLG undergoes an electronic topological transition, where four Dirac cones around the Fermi level reduces to two Dirac cones with equal or unequal Dirac energies depending on the shift direction. While the critical electric field required for the band gap opening increases with increasing lateral shift for the two Dirac cones with unequal Dirac energies, the critical field is essentially zero even with a lateral shift for the two Dirac cones with equal Dirac energies. The critical field is determined by the Dirac energy difference and the electronic screening effect. The massless helical and the massive chiral fermions are believed to be responsible for perfect and imperfect electronic screening effect, respectively.

Methods

A Bernal-stacked BLG was considered as a two-dimensional system with a lattice constant $a = 2.46 \text{ \AA}$ and an interlayer distance $d_o = 3.35 \text{ \AA}$. For sliding BLG, the interlayer distance was taken from a previous work¹. Our DFT calculations were carried out without considering the Van der Waals interaction. However, while the Van der Waals interaction between graphene layers plays an important role in determining the interlayer distance¹, the electronic properties are little affected by it as would be our results^{7,9}. The vacuum spacing between the BLGs was set to 20 \AA . As usual, the z axis was taken along the direction perpendicular to the layer. A Quantum Espresso package, using plane waves as the basis set for wave functions, was employed for the DFT calculation²⁵. Norm-conserving fully-relativistic pseudopotentials²⁶ and a generalized gradient approximation (GGA) of Perdew-Burke-Ernzerhof (PBE)²⁷ form for the exchange-correlation (XC) potential were used. Based on the stable charge density obtained from self consistent field (SCF) calculations with a kinetic energy cutoff of 250 Ry and k -points of $48 \times 48 \times 1$ mesh, the wavefunctions were obtained with k -points of $24 \times 24 \times 1$ mesh. Some calculations were done with k -points of $96 \times 96 \times 1$ mesh for SCF calculations and $48 \times 48 \times 1$ mesh for wavefunctions to check for the reliability. A periodic sawtooth potential was used to simulate the external electric field. Using the wavefunctions obtained from the DFT calculations, relativistic maximally localized Wannier functions were constructed within the Wannier90 code²⁸. Based on the Wannier interpolation, all the electronic properties such as the density of states were calculated.

References

1. Son, Y.-W., Choi, S.-M., Hong, Y. P., Woo, S. & Jhi, S.-H. Electronic topological transition in sliding bilayer graphene. *Phys. Rev. B* **84**, 155410 (2011).
2. Brown, L. *et al.* Twinning and twisting of tri- and bilayer Graphene. *Nano Lett.* **12**, 1609 (2012).
3. Hattendorf, S., Georgi, A., Liebmann, M. & Morgenstern, M. Networks of ABA and ABC stacked graphene on mica observed by scanning tunneling microscopy. *Surf. Sci.* **610**, 53–58 (2013).
4. Alden, J. S. *et al.* Strain solitons and topological defects in bilayer graphene. *Proc. Natl. Acad. Sci.* **110**, 11256–11260 (2013).
5. Feng, X., Kwon, S., Park, J. Y. & Salmeron, M. Superlubric sliding of graphene nanoflakes on graphene. *ACS Nano* **7**, 1718 (2013).
6. Chang, S.-L., Wu, B.-R., Wong, J.-H. & Lin, M.-F. Configuration-dependent geometric and electronic properties of bilayer graphene nanoribbons. *Carbon* **77**, 1031–1039 (2014).
7. Min, H., Sahu, B., Banerjee, S. K. & MacDonald, A. H. *Ab initio* theory of gate induced gaps in graphene bilayers. *Phys. Rev. B* **75**, 155115 (2007).
8. Castro, E. V. *et al.* Biased bilayer graphene: Semiconductor with a gap tunable by the electric field effect. *Phys. Rev. Lett.* **99**, 216802 (2007).
9. Gava, P., Lazzeri, M., Saitta, A. M. & Mauri, F. *Ab initio* study of gap opening and screening effects in gated bilayer graphene. *Phys. Rev. B* **79**, 165431 (2009).
10. McCann, E. Asymmetry gap in the electronic band structure of bilayer graphene. *Phys. Rev. B* **74**, 161403(R) (2006).
11. Choi, S.-M., Jhi, S.-H. & Son, Y.-W. Anomalous optical phonon splittings in sliding bilayer graphene. *ACS Nano* **7**, 7151–7156 (2013).
12. Tran, N. T. T., Lin, S.-Y., Glukhova, O. E. & Lin, M.-F. Configuration-induced rich electronic properties of bilayer graphene. *J. Phys. Chem. C* **119**, 10623–10630 (2015).
13. McCann, E. & Koshino, M. The electronic properties of bilayer graphene. *Rep. Prog. Phys.* **76**, 056503 (2013).
14. Kunschuh, S., Gmitra, M., Kochan, D. & Fabian, J. Theory of spin-orbit coupling in bilayer graphene. *Phys. Rev. B* **85**, 115423 (2012).
15. Oostinga, J. B., Heersche, H. B., Liu X., Morpurgo, A. F. & Vandersypen, L. M. K. Gate-induced insulating state in bilayer graphene devices. *Nature Mater.* **7**, 151–157 (2008).
16. Mayorov, A. S. *et al.* Interaction-driven spectrum reconstruction in bilayer graphene. *Science* **333**, 860–863 (2011).
17. Velasco Jr., J. *et al.* Transport spectroscopy of symmetry-broken insulating states in bilayer graphene. *Nat. Nanotechnol.* **7**, 156–160 (2012).
18. Weitz, R. T., Allen, M. T., Feldman, B. E., Martin, J. & Yacoby, A. Broken-symmetry states in doubly gated suspended bilayer graphene. *Science* **330**, 812–816 (2010).
19. Sui, M. *et al.* Gate-tunable topological valley transport in bilayer graphene. *Nature Phys.* doi: 10.1038/NPHYS3485 (2015).
20. Qiao, Z. *et al.* Topological phases in gated bilayer graphene: Effects of Rashba spin-orbit coupling and exchange field. *Phys. Rev. B* **87**, 125405 (2013).
21. Guo, Y., Guo, W. & Chen, C. Tuning field-induced energy gap of bilayer graphene via interlayer spacing. *Appl. Phys. Lett.* **92**, 243101 (2008).
22. Choi, S.-M., Jhi, S.-H. & Son, Y.-W. Controlling Energy Gap of Bilayer Graphene by Strain. *Nano Lett.* **10**, 3486–3489 (2010).
23. Kim, K. S. *et al.* Coexisting massive and massless Dirac fermions in symmetry-broken bilayer graphene. *Nature Mater.* **12**, 887–892 (2013).
24. Park, C. *et al.* Electronic Properties of Bilayer Graphene Strongly Coupled to Interlayer Stacking and an External Electric Field. *Phys. Rev. Lett.* **115**, 015502 (2015).
25. Giannozzi, P. *et al.* QUANTUM ESPRESSO: a modular and open-source software project for quantum simulations of materials. *J. Phys.: Condens. Matter* **21**, 395502 (2009).

26. Troullier, N. & Martins, J. L. Efficient pseudopotentials for plane-wave calculations. II. Operators for fast iterative diagonalization. *Phys. Rev. B* **43**, 8861–8869 (1991).
27. Perdew, J. P., Burke, K. & Ernzerhof, M. Generalized gradient approximation made simple. *Phys. Rev. Lett.* **77**, 3865–3868 (1996).
28. Mostofi, A. A. *et al.* wannier90: A tool for obtaining maximally-localised Wannier functions. *Comput. Phys. Commun.* **178**, 685–699 (2008).

Acknowledgements

This work was supported by the National Research Foundation of Korea (Project No. 2013057555, 2015M1A7A1A01002234, NRF-2010-0027963, and 2015M2B2A4029012).

Author Contributions

K.W.L. initiated the study, performed D.F.T. calculations, and analyzed data. C.E.L. supervised the project. K.W.L. and C.E.L. wrote the manuscript.

Additional Information

Competing financial interests: The authors declare no competing financial interests.

How to cite this article: Lee, K. W. and Lee, C. E. Extreme sensitivity of the electric-field-induced band gap to the electronic topological transition in sliding bilayer graphene. *Sci. Rep.* **5**, 17490; doi: 10.1038/srep17490 (2015).



This work is licensed under a Creative Commons Attribution 4.0 International License. The images or other third party material in this article are included in the article's Creative Commons license, unless indicated otherwise in the credit line; if the material is not included under the Creative Commons license, users will need to obtain permission from the license holder to reproduce the material. To view a copy of this license, visit <http://creativecommons.org/licenses/by/4.0/>